

See discussions, stats, and author profiles for this publication at: <https://www.researchgate.net/publication/23266466>

Transformation of Reactive Iron Minerals in a Permeable Reactive Barrier (Biowall) Used to Treat TCE in Groundwater

ARTICLE *in* ENVIRONMENTAL SCIENCE AND TECHNOLOGY · OCTOBER 2008

Impact Factor: 5.33 · DOI: 10.1021/es8010354 · Source: PubMed

CITATIONS

20

READS

70

3 AUTHORS, INCLUDING:



Thomas He

West Virginia University

24 PUBLICATIONS 395 CITATIONS

[SEE PROFILE](#)



John T Wilson

United States Environmental Protection A...

143 PUBLICATIONS 3,908 CITATIONS

[SEE PROFILE](#)

Transformation of Reactive Iron Minerals in a Permeable Reactive Barrier (Biowall) Used to Treat TCE in Groundwater

Y. THOMAS HE,*† JOHN T. WILSON, AND RICHARD T. WILKIN

U.S. Environmental Protection Agency, National Risk Management Research Laboratory, Ground Water and Ecosystems Restoration Division, 919 Kerr Research Drive, Ada, Oklahoma 74820

Received April 25, 2008. Revised manuscript received June 18, 2008. Accepted June 18, 2008.

Iron and sulfur reducing conditions generally develop in permeable reactive barrier systems (PRB) constructed to treat contaminated groundwater. These conditions allow formation of FeS mineral phases. FeS readily degrades TCE, but a transformation of FeS to FeS₂ could dramatically slow the rate of TCE degradation in the PRB. This study uses acid volatile sulfide (AVS) and chromium reducible sulfur (CRS) as probes for FeS and FeS₂ to investigate iron sulfide formation and transformation in a column study and PRB field study dealing with TCE degradation. Solid phase iron speciation shows that most of the iron is reduced and sulfur partitioning measurements show that AVS and CRS coexist in all samples, with the conversion of AVS to CRS being most significant in locations with potential oxidants available. In the column study, 54% of FeS was transformed to FeS₂ after 2.4 years. In the field scale PRB, 43% was transformed after 5.2 years. Microscopy reveals FeS, Fe₃S₄ and FeS₂ formation in the column system; however, only pyrite formation was confirmed by X-ray diffraction. The polysulfide pathway is most likely the primary mechanism of FeS transformation in the system, with S⁰ as an intermediate species formed through H₂S oxidation.

Introduction

Previous studies on abiotic reduction of chlorinated solvents have examined different iron minerals, including Fe(0) (1), Fe(II) sorbed to iron oxides (2), green rust (3), magnetite (4), and iron sulfides (5, 6), and almost all of these studies are conducted in laboratory batch studies with synthesized materials. There are a few field related studies providing evidence that iron sulfides have an important contribution to the degradation of chlorinated solvents in natural and engineered systems (7, 8).

Permeable reactive barrier (PRB) technology is commonly used to treat groundwater contamination for both organic and inorganic contaminants (9–13). Both iron and sulfate are abundant in groundwater environments. Under the sulfur and iron reducing conditions typically encountered in PRB systems, the formation of various FeS phases would be expected, and FeS precipitation has been reported in several

reactive barrier systems (10, 12, 13). Amorphous FeS and poorly crystalline mackinawite (tetragonal structure) have been observed in PRB systems constructed with zerovalent iron (ZVI) and in biowall systems constructed with plant mulch (12, 13). However, iron mineralogy in these systems is not well characterized. This is partly due to the fact that it is difficult to positively identify FeS phases using X-ray diffraction (XRD) and microscopic techniques in these complex sediment and soil samples (12). A field study by Herbert et al. (10) demonstrated the inability to identify iron sulfide minerals from reactive media by either XRD or scanning electron microscopy (SEM), and formation of FeS was identified only on piezometer tubing. In this study, FeS phases were directly identified by XRD and SEM in the reactive material of column and field samples.

In 2002, a biowall composed of sand and plant mulch was constructed at Altus Air Force Base, OK to treat a TCE plume in groundwater. A column study was conducted to simulate field conditions at Altus AFB in order to better understand the mechanisms responsible for removal of TCE (9). Removal of TCE is extensive (>92–99%) in both the biowall and the column experiments (9, 14). However, the mechanism for TCE degradation in these systems is only partially understood. Based on the extent of sulfate reduction, FeS formation in the columns could be estimated, and Shen and Wilson (9) concluded that TCE removal associated with FeS could account for about one-half of TCE degradation in the column experiment. Acetylene and ¹³C labeled CO₂ constituted the major products from abiotic reduction of ¹³C labeled TCE (9). Butler and Hayes (6) showed that TCE can be degraded by FeS through a reductive elimination pathway, producing acetylene as a major reaction product. Acetylene is a signature of abiotic reduction.

Amorphous or poorly crystalline FeS is more effective than FeS₂ in degrading TCE (15, 16). To predict the long-term ability of a PRB to remove TCE, it is necessary to have a better understanding of the processes that form FeS and the processes that transform FeS to FeS₂ in PRBs. We used acid volatile sulfide (AVS) and chromium reducible sulfur (CRS) as probes for FeS formation and transformation to FeS₂, and applied XRD and microscopy techniques to elucidate the biogeochemical processes that are relevant to FeS formation and transformation in a PRB.

Materials and Methods

Background. Figure 1a shows the location of the OU-1 biowall which was constructed to treat a TCE groundwater plume at Altus AFB, OK. It is 138.7 m long, 7.3 m deep, and 0.46 m wide. It contains a blend of 50% (v/v) shredded tree mulch, 10% (v/v) cotton gin trash, and 40% (v/v) sand. On a volume basis, the biowall averages 71% solids and 29% water. The estimated residence time of groundwater in the biowall is 10 days.

Shen and Wilson (9) constructed Column B3 (Figure 1b) using the same materials as the OU-1 biowall, with the following exception. While the biowall was constructed with 40% sand, Column B3 contained 36% sand and 4% hematite. Hematite was added to Column B3 to determine the benefit of adding a source of reactive Fe(III) in future biowalls. Shen and Wilson (9) had constructed four columns simulating a plant mulch biowall. Based on a mass balance of sulfate entering the columns and sulfate and sulfide leaving the columns, Column B3 had accumulated the highest concentration of FeS. Column B3 was selected for a detailed characterization of the fractionation of iron and sulfur mineral phases.

* Corresponding author phone: 580-436-8554; fax: 580-436-8703; e-mail: he.yongtian@epa.gov.

† National Research Council.

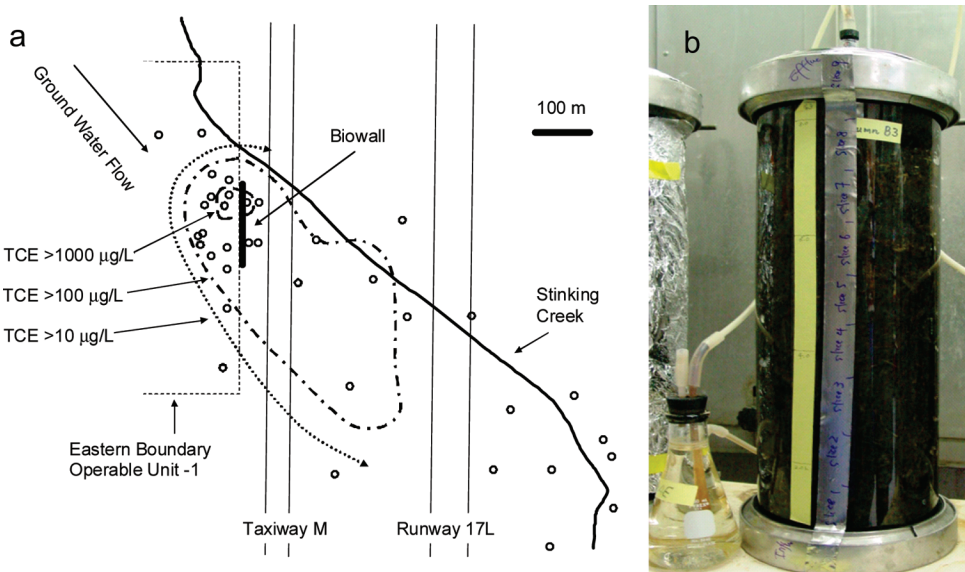


FIGURE 1. (a) Location of a PRB (a biowall) constructed at Altus AFB in June 2002. (b) Column B3 constructed to simulate field conditions in the OU-1 biowall.

The column was supplied with groundwater from Altus AFB amended with TCE to a final concentration of $15 \mu\text{M}$. The water was pumped upward from the inlet at the bottom of the column with a peristaltic pump. The mean residence time of groundwater in the column was 17 days. The chemical composition of materials used to construct Column B3 and the field scale OU-1 biowall are listed in Table S1 and S2 in the Supporting Information (SI).

Groundwater and Solid Phase Sampling. Procedures for sampling and for chemical analysis of water samples are described in the SI. Figure S1 in the SI shows the locations of monitoring wells at the OU-1 site at Altus AFB.

After 875 days of operation, Column B3 was put into a freezer for 1 week. This was done to immobilize the contents of the column and protect them from oxidation during exposure to the atmosphere, and to break the glass container away from the frozen column of plant mulch, sand, and groundwater. The broken glass was discarded and the column was cut while still frozen into 5 cm thick sections using a hand saw. Each section was thawed in an anaerobic glovebox ($\text{N}_2:\text{H}_2 = 92.5\%:7.5\%$), homogenized and separated into four equal subsections and refrozen until analysis. Samples that were extracted and analyzed to determine iron and sulfur partitioning were thawed in the glovebox in sealed containers. Wet sediments were used directly for analysis and corrected for H_2O content. H_2O content was determined gravimetrically. For total sulfur measurement, samples were dried inside the glovebox.

To acquire samples of the OU-1 biowall, a freeze core sampling technique was developed. This technique used liquid N_2 to freeze mulch material in the biowall in situ. Mulch materials were then retrieved as a "Popsicle" (Figure S2 in SI). Each core collected from the subsurface was immediately wrapped in a plastic bag and placed on dry ice in an ice chest. Further sample preparation for iron and sulfur analysis followed the same procedure as the column samples.

Iron and Sulfur Partitioning. The iron partitioning procedure was modified after Kosta and Luther (17). For sulfur partitioning, the extraction and experimental setup followed procedures in Wilkin and Bischoff (18). Table 1 provides the details of each extraction step and the targeted iron mineral phases.

Solid Phase Characterization. X-Ray diffraction (XRD) scans were collected with a Rigaku MiniFlex diffractometer (Fe $\text{K}\alpha$ radiation, operated at 30 keV and 15 mA). As a preconcentration step to prepare XRD samples, mulch

materials were washed with methanol, and large sand particles and splinters of mulch were removed. A fine-grained fraction was collected using a $0.4 \mu\text{m}$ filter and dried in a vacuum desiccator.

Scanning electron microscope (SEM) images were obtained using a JEOL JSM-6360 scanning electron microscope with EDS/Oxford INCA software. SEM samples were prepared by placing a drop of methanol suspension of mulch on a carbon planchet (Electron Microscopy Sciences). The planchet was placed in a vacuum desiccator to dry overnight, and then coated with gold prior to SEM examination.

Equilibrium geochemical modeling software (Geochemist's Workbench, Release 6.0, Rockware, Golden, CO) was used to model groundwater chemical speciation. Model simulations considered the formation of solution complexes and precipitation of solids. The solubility model of Rickard (19) was used to calculate saturation indices of FeS.

Results and Discussion

Groundwater Chemistry. The operating conditions for Column B3 simulated groundwater conditions at the OU-1 biowall of Altus AFB. Typical chemical compositions of influent and effluent from Column B3 are shown in Table S3 in the SI. In general, the column effluent contained lower concentrations of dissolved oxygen (DO) and sulfate and higher concentrations of dissolved sulfide and alkalinity compared to the influent. Alkalinity was increased due to CO_2 production during biodegradation of the plant mulch. In column B3, concentrations of sulfide was never higher than 16 mg/L. Typical composition of groundwater at the Altus biowall field site is shown in Table S4 in the SI. Inside the biowall, sulfide concentrations range from 60 to 220 mg/L depending on location.

Hematite was not added during construction of the field scale OU-1 biowall. There was a limited amount of iron in the sand added to the mulch material, and as a result the potential for FeS formation in the OU-1 biowall was significantly lower than in Column B3, which explains the higher concentrations of sulfide measured in groundwater in the field compared to the effluent of Column B3. The H_2S concentrations in the system are controlled by bacterial sulfate reduction and the availability of reactive iron.

Geochemical modeling indicates that groundwater within the biowall is near saturation with respect to iron monosulfide. Mean saturation indices for crystalline mackinawite and disordered mackinawite are 0.38 and -0.41 , respectively

TABLE 1. Extraction Methods Used to Characterize the Fractionation of Iron and Sulfur Species in the Samples

extraction	extractants	pH	time	target mineral phases
iron extraction procedure modified after Kostka and Luther (17).				
ascorbate	10 mL extractant composed of 0.17 M sodium citrate (Aldrich), 0.60 M sodium bicarbonate (Fisher) and 0.11 M ascorbic acid (Fisher)	8	24 h	amorphous iron oxides
HCl	10 mL 0.5 M HCl (J.T.Baker)	<2.0	1 h	amorphous iron oxides, AVS
dithionite	10 mL extractant composed of 0.29 M sodium dithionite (Fisher), 0.35 M sodium acetate (J.T.Baker) and 0.2 M sodium citrate at 60 °C	4	4 h	amorphous iron oxides, crystalline iron oxides, AVS
HNO ₃	Microwave digestion at 175 °C in 10% HNO ₃ (JT Baker)		0.5 h	total iron
Sulfur fractionation procedure after Wilkin and Bischoff (18)				
AVS	1 M HCl (J.T. Baker)			amorphous FeS, mackinawite, greigite
CRS	1 M CrCl ₂ in 0.5 M HCl, Prepared by passing 1 M CrCl ₃ ·6H ₂ O (Fluka, 98+%) dissolved in 0.5 M HCl through a standard Jones redactor			elemental S, pyrite
Total sulfur	V ₂ O ₅ (Aldrich, 98+%), sample combusted in two furnaces aligned in sequence (UIC model CM3220)			AVS, CRS, SO ₄ ²⁻

(n = 17). These results indicate that geochemical modeling based on water chemistry parameters is useful in evaluating whether reactive mineral phases might be present at sites under situations where solids cannot be collected and directly analyzed for reactive mineral phases.

Solid Phase Iron Fractionation. Figure 2 presents data on iron partitioning in Column B3 and in core samples from the OU-1 mulch biowall. Iron extracted by ascorbate includes amorphous Fe(III) oxides. The concentration of iron extractable by ascorbate was negligible. Iron extracted by HCl includes both amorphous Fe(III) oxides and iron associated with AVS. The low concentration of iron extracted by ascorbate and the high concentration of iron extracted by HCl in material from Column B3 suggests that almost all the iron was reduced under anaerobic conditions in the column after 875 days of continuous operation. The low concentration of iron extacted by HCl in the biowall samples suggests that the original pool of available reactive iron was small compared with Column B3. Dithionite extracts amorphous Fe(III)

oxides, crystalline Fe(III) oxides and iron associated with AVS. Measured concentrations of iron extracted with HCl or with dithionite are very similar across the column and OU-1 field samples, which indicates that there are only trace amounts of crystalline Fe(III) oxides remaining in these materials. Total iron was measured as iron extracted by HNO₃ during microwave digestion. In the biowall samples and the few sections of Column B3 that are further down gradient of the inlet, the concentration of total iron is significantly higher than iron that was extacted by HCl or dithionite. Total iron includes the FeS₂ fraction, which is not extracted by HCl or dithionite.

Reactive iron has traditionally been defined as that fraction of iron in sediments which reacts readily with sulfide to form iron sulfides and pyrite (17, 20). The iron which may react with H₂S (reactive iron) is mainly iron that is not bound in silicate minerals, including amorphous iron (oxyhydr)oxides, some crystalline iron oxides, and iron monosulfides. Operationally, reactive iron has been defined as iron extracted

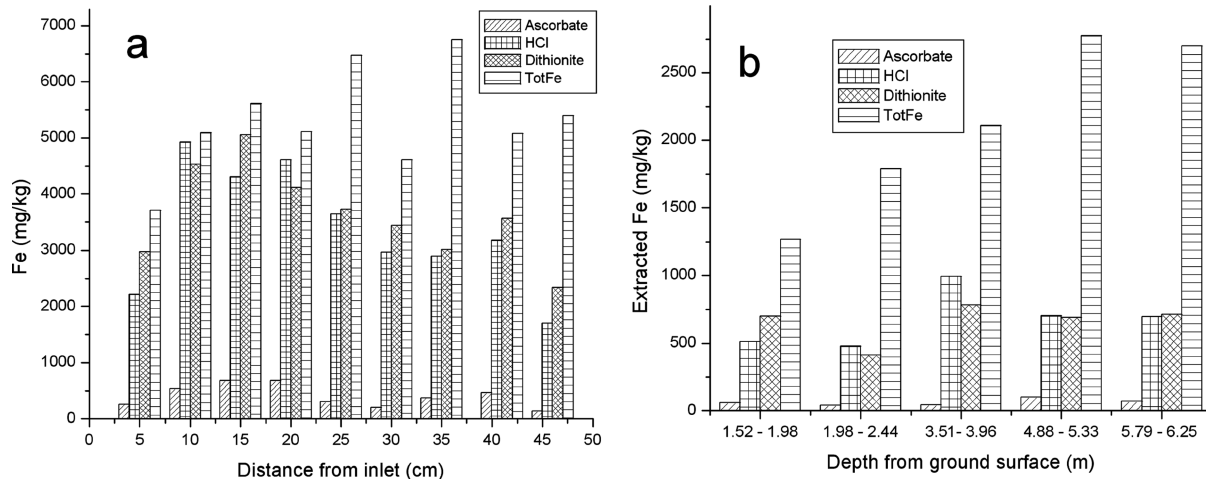


FIGURE 2. Iron fractionation in sections of Column B3 and core samples from the OU-1 biowall. (a) column B3, (b) OU-1 field samples.

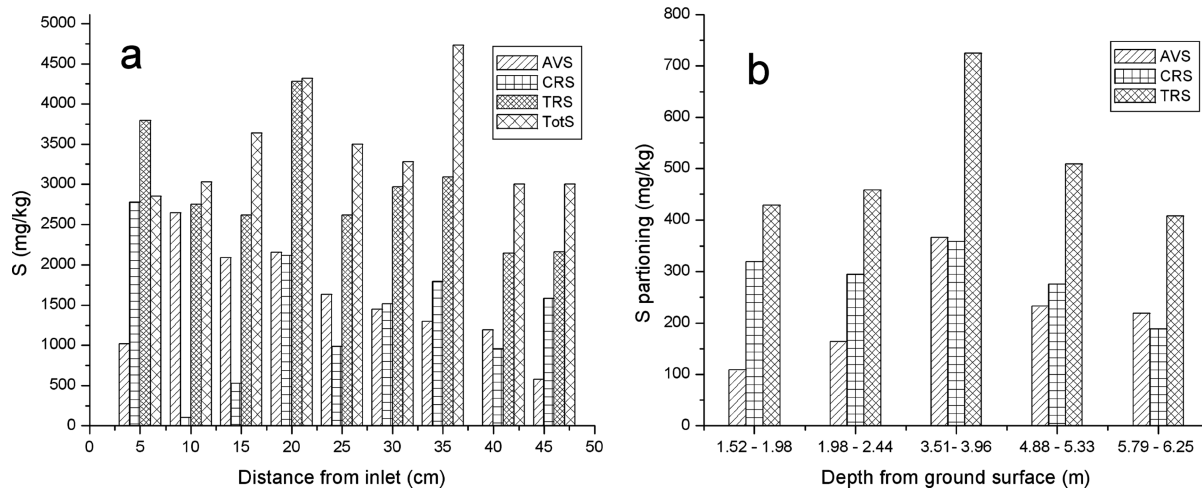


FIGURE 3. Sulfur fractionation in sections of Column B3 and core samples from the OU-1 biowall. (a) Column B3, (b) OU-1 biowall.

by HCl (21). In the OU-1 biowall, the pool of remaining reactive iron is small compared to the pool of total iron, between 480 and 1000 mg/kg of reactive iron compared to 1270 to 2780 mg/kg total iron. In Column B3, the pool of reactive iron is large compared to the biowall, extending from 1700 to 4930 mg/kg in Column B3, compared to 480 and 1000 mg/kg in the biowall.

Solid Phase Sulfur Fractionation. AVS can form during reductive dissolution of iron hydroxides or by reaction of ferric iron in clay minerals during reduction with sulfide (22). AVS is operationally defined as reduced inorganic sulfur that reacts with HCl to form H₂S gas (23). The AVS procedure employed in this study was intended to digest labile sulfide compounds; it recovers sulfide in pore water and solid-phase sulfide minerals, which include amorphous FeS, mackinawite (FeS_{0.9-1.1}) and greigite FeS_{1.33} (Fe₃S₄) (23, 24).

The CRS fraction has been defined as sulfide phases that are not extractable in HCl over short time-frames (25). The CRS extraction procedure (by CrCl₂-HCl) is intended to digest refractory sulfur-bearing compounds, such as pyrite/marscasite (FeS₂) and elemental sulfur (S⁰).

Figure 3a shows the relative distribution of AVS, CRS, total reduced sulfur (TRS, TRS = AVS + CRS) and total sulfur at each section of Column B3. CRS is high in the influent section (>2000 mg/kg). There is little CRS in the 10–15 cm segment, and CRS increases in upper sections (20–46 cm). In these sections, AVS and CRS seem to be inversely correlated.

Figure 3b shows sulfur partitioning across depths of the biowall at the Altus field site. Compared to Column B3, measured AVS and CRS concentrations in the Altus biowall are much lower.

The low concentration of solid phase sulfide suggests that the low concentrations of reactive iron in the sediment limited FeS formation. In shallow depths of 1.52–1.98 m and 1.98–2.44 m, the CRS/AVS ratio is higher than samples from deeper depths (>3.51 m). At deeper depths, less AVS is transformed to CRS. Even though the sulfide concentration inside the wall is high, it apparently does not precipitate as elemental S or form other intermediate sulfur species due to lack of available oxidants (presumably dissolved O₂) at deeper depths. These intermediate species are believed to be essential in the transformation of AVS (FeS) to CRS (FeS₂).

Sulfur partitioning in column and field samples show that AVS and CRS coexist, but the ratio of AVS/CRS is related to local and micro geochemical conditions. Over time, sedimentary AVS tends to be replaced by the thermodynamically more favorable CRS fraction (pyrite) (23). Rickard and others (26) have shown that the kinetics of iron monosulfide precipitation are fairly rapid, whereas the transformation of a FeS precursor phase to pyrite is a slower process.

Concentrations of AVS and CRS in Column B3 are inversely related. This suggests that at least part of the CRS is produced from AVS. Previous studies suggest that the conversion of AVS to CRS occurs mostly at redox boundaries where an oxidant (e.g., O₂) is available (27). This is consistent with our observations in the column experiments, that transformation of AVS to CRS was more extensive in the influent end of the column where potential oxidants such as dissolved oxygen were available.

Based on the sulfur partitioning data (Figure 3), and the assumption that all the CRS in the samples was originally AVS, it is possible to calculate the extent of transformation of AVS to CRS in the samples. Data are presented in Tables S5 and S6 in the SI. In the biowall samples, from 55 to 58% of the sulfide remains as AVS. In the sections of Column B3, from 87 to 19% of the sulfide remains as AVS, with an average of 45%. Within 5.2 years for the biowall, and 2.4 years for Column B3, roughly one-half of the reactive FeS was transformed to the much less reactive FeS₂. The estimated rate of transformation of AVS to CRS in the influent section of Column B3 is 1.5×10^{-3} mol kg⁻¹ d⁻¹, which is similar to a transformation rate reported by Canfield et al. (28). They suggested bacteria in these systems could play a role in the process of conversion of FeS (AVS) to FeS₂ (CRS).

Mineralogical Characteristics. Mineralogy of the biowall material in column experiments and field core samples was characterized by XRD and SEM/EDX. In the coarse sediment samples, quartz dominates the sediment mineralogy. In methanol washed samples, in addition to quartz, pyrite was identified by both XRD and SEM, and residual hematite was observed in Column B3 samples (Figure 4, and SI Figure S3 and S4).

Under anaerobic conditions, formation of amorphous iron sulfide and mackinawite could occur as finely dispersed precipitates and as coatings on hematite and other minerals (23). FeS formation was not confirmed by XRD, but is identifiable by EDX based on chemical composition in Column B3 samples. The EDX data show that the metastable iron sulfides have a chemical composition of FeS_{0.9-1.4}, and probably represent a mixture of stoichiometric mackinawite and greigite. The FeS/greigite morphology (Figure 4b) is similar to chemically synthesized FeS (unpublished data, He et al.). This noncrystalline FeS is generally the first phase of FeS to precipitate. In heterogeneous mixtures, it is difficult to positively identify FeS minerals with XRD due to low crystallinity of the FeS phases. Contrary to the experience with the samples from Column B3, FeS or greigite phases could not be identified in the field sediments by either XRD or SEM/EDX.

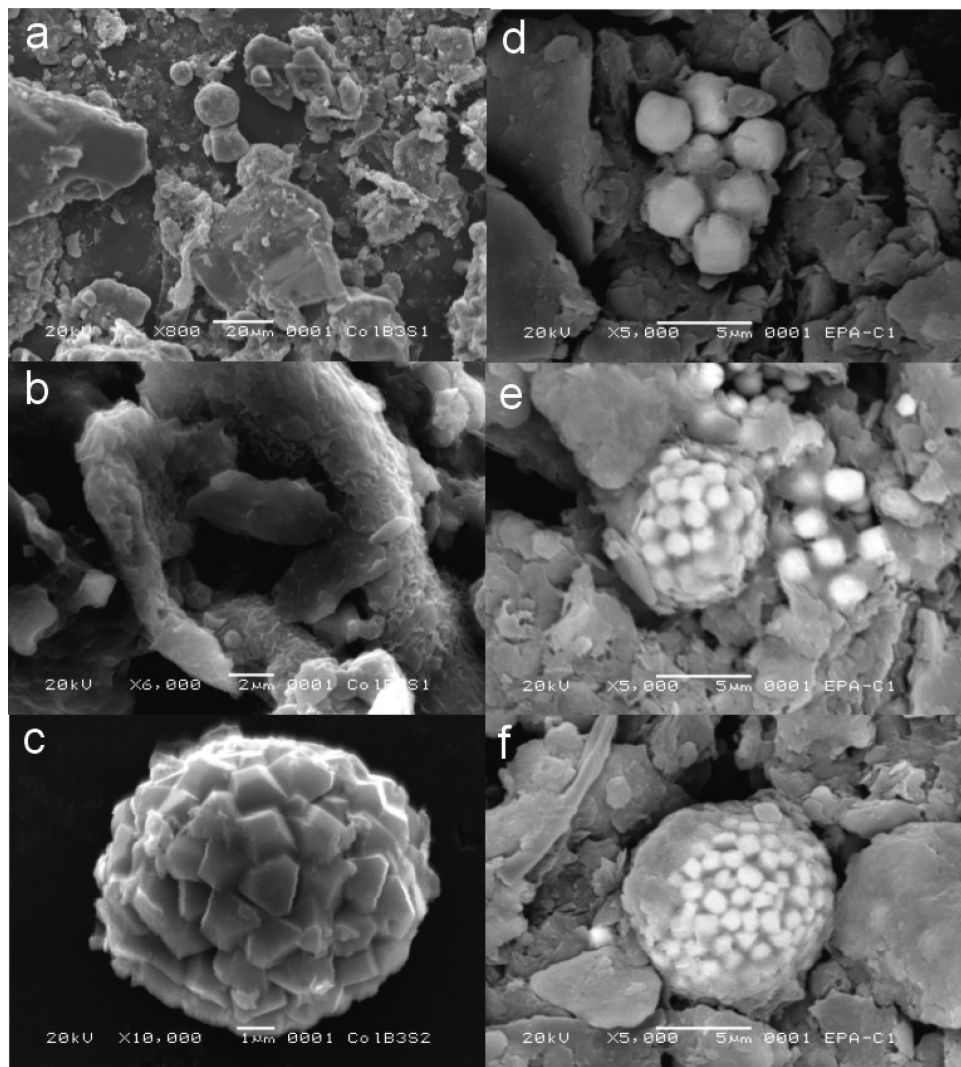


FIGURE 4. SEM of Column B3 samples. (a). Hematite, FeS, and FeS₂ particles; b) FeS, (c) pyrite framboids. d, e, and f are backscattered electron images of the OU-1 biowall samples. (d) framboids showing no clear microcrystals; (e) framboid and dispersed microcrystals; (f) pyrite framboid with surface coating.

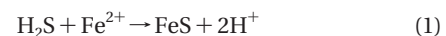
Pyrite was the only FeS phase confirmed by XRD, and EDX analysis of the reaction products returned Fe:S ratios (1:2) consistent with FeS₂ stoichiometry. SEM showed different morphologies of pyrite framboids (Figure 4 and Figure S5 in the SI). Some framboids show unordered microcrystal arrangement, other framboids show different shapes of microcrystals (triangular, round and rectangular), and framboids are present in random sizes. Framboid diameter size ranges from about 6 to 20 μm . Butler and Rickard (29) suggest that differences in framboid morphology could be related to formation kinetics. In the OU-1 field samples, SEM also shows organic coatings formed on framboid surfaces. This could be an indication that bacteria play a role in pyrite framboid formation.

Iron Sulfide Formation and Transformation.

FeS Formation. In the OU-1 biowall and in the column experiments, sulfate reduction is mediated by sulfate reducing bacteria (SRB) under anaerobic conditions. Accompanying sulfate reduction in the system, reductive dissolution of hematite and other iron oxides can occur through two pathways: dissimilatory iron reduction by iron reducing bacteria and reductive dissolution of hematite by hydrogen sulfide (22).

In the column experiment and the OU-1 biowall, measured sulfide concentrations range from 6 to 228 mg/L. The production of dissolved sulfide species in the presence of

dissolved metals can result in precipitation of metal sulfide mineral phases such as FeS.

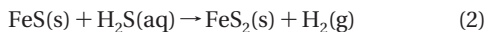


Other metals such as Mn, Ni, and Zn, can also be released to groundwater under iron and sulfur reducing conditions, and can react with sulfide to form sparingly soluble sulfide minerals. SEM/EDX showed NiS and ZnS formation in the system, but they are only minor components compared to FeS because there were only trace amounts of these elements potentially available to react with sulfide (Table S2 in the SI).

Transformation of FeS to FeS₂. FeS is redox sensitive and metastable in the environment. It may be transformed to FeS₂ based on several different mechanisms. A polysulfide pathway is proposed to be the primary pathway for formation of FeS₂(s) in suboxic sediments. In this process iron sulfide precursors react with S⁰, polysulfides or other sulfur intermediates to form pyrite. Production of intermediate sulfur species (for example, elemental sulfur, polysulfides and thiosulfates (S₂O₃²⁻)) is initiated through H₂S oxidation near the redox boundary by oxidants such as O₂, NO₃⁻, and iron oxides and manganese oxides (29, 30). Transformation via reaction with elemental sulfur is most likely the dominant pathway in our systems based on the observation that greater

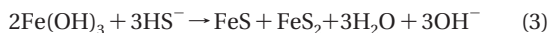
conversion to CRS occurred only in sections of Column B3 where potential oxidants are available.

Under strictly anoxic conditions, FeS₂(s) has also been shown to form via a second mechanism, the “H₂S oxidation pathway” (26, 31).



Rickard and Luther (31) show the H₂S pathway to proceed more rapidly than the polysulfide pathway and all other pathways involving intermediate sulfur species. High sulfide concentration in the field and column is conducive to this mechanism.

A third mechanism, the “direct” pyrite precipitation pathway, could occur through prolonged exposure of iron-containing minerals to dissolved sulfide. Pyrite originates from exposure of iron(II)-containing minerals to dissolved sulfide and most likely precipitates on a pyrite precursor (“seed”) without the formation of a FeS_n precursor (30). The direct pyrite formation from iron oxides may be described by the following reaction (18):



For the first pathway, intermediate sulfur species are critical in pyrite formation. Thus the availability of an oxidant to produce sulfur species with intermediate oxidation states controls the transformation of FeS to pyrite. The transformation of FeS to FeS₂ is most pronounced at the redox interface in our systems. The conversion of iron monosulfides to pyrite in Column B3 occurs in the section adjacent to the inlet as well as the down gradient parts of the columns, and an increase in CRS is accompanied by a decrease in AVS. Higher levels of CRS in the section adjacent to the inlet could be due to dissolved O₂ in the influent. Water analyses in Column B3 showed that dissolved O₂ level is greatly reduced in the effluent, presumably consumed in the bottom section of Column B3. The increased CRS concentration in the middle and far down gradient sections of the column could be due to high concentrations of S⁰ in the down gradient sections, which facilitated pyrite formation. In a PRB field study, Herbert (10) observed a greater accumulation of mildly oxidized sulfur species (pyrite, S₀) at the front end of the barrier. This observation suggests that oxidizing agents may be present in the upgradient aquifer in low concentrations, but are consumed as groundwater passes through the reactive barrier.

Implications. The formation of reactive FeS is important to the degradation of chlorinated solvents in permeable reactive barriers. Shen and Wilson (9) show that abiotic transformation of TCE by FeS could provide a major contribution to the removal of TCE from the groundwater at the Altus AFB. Abiotic degradation of TCE associated with FeS may have an important role in many natural attenuation and engineered remedies.

FeS is metastable and will transform to more stable FeS₂ over time. FeS to FeS₂ transformation in biowalls could potentially reduce the rate of TCE degradation. Weerasooriya and Dharmasena (15) show FeS₂ is much less efficient in TCE degradation (15–66 times slower). Lee and Batchelor (16) indicated that pyrite degraded TCE at a rate >1000 times slower than FeS. Thus the pyritization process observed in the column and field experiments in this study can significantly decrease the extent of degradation of TCE in PRBs.

A supply of reactive iron in the matrix of the biowall will stimulate the formation of FeS. This FeS will promote the abiotic dechlorination pathway (5, 6), as opposed to biological reductive dechlorination. In the abiotic degradation pathway, much of the TCE is degraded to acetylene, which avoids any potential for the formation of vinyl chloride, which is a major intermediate in biological degradation.

Engineered systems that are designed to exploit abiotic degradation will be most successful when the concentrations of naturally occurring reactive iron are high or when supplemental reactive iron is introduced to the subsurface.

Acknowledgments

The U.S. Environmental Protection Agency through its Office of Research and Development funded the research described here. It has not been subjected to Agency review and therefore does not necessarily reflect the views of the Agency, and no official endorsement should be inferred. Y.T. He is an associate of the National Research Council.

Supporting Information Available

Additional information on sampling and analysis of groundwater, location of monitoring wells, XRD data, SEM micrographs, chemical composition of materials used for construction of the biowall and the laboratory column, geochemical parameters in water from the column and the biowall, and the iron and sulfur fractionation in samples from the column and biowall. This material is available free of charge via the Internet at <http://pubs.acs.org>.

Literature Cited

- (1) Arnold, W. A.; Roberts, A. L. Pathways and kinetics of chlorinated ethylene and chlorinated acetylene reaction with Fe(0) particles. *Environ. Sci. Technol.* **2000**, *34*, 1794–1805.
- (2) Amonette, J. E.; Workman, D. J.; Kennedy, D. W.; Fruchter, J. S.; Gorby, Y. A. Dechlorination of carbon tetrachloride by Fe(II) associated with goethite. *Environ. Sci. Technol.* **2000**, *34*, 4606–4613.
- (3) Lee, W.; Batchelor, B. Abiotic reductive dechlorination of chlorinated ethylenes by iron-bearing soil minerals. 2. Green rust. *Environ. Sci. Technol.* **2002**, *36*, 5348–5354.
- (4) Danielsen, K. M.; Hayes, K. F. pH dependence of carbon tetrachloride reductive dechlorination by magnetite. *Environ. Sci. Technol.* **2004**, *38*, 4745–4752.
- (5) Butler, E. C.; Hayes, K. F. Kinetics of the transformation of trichloroethylene and tetrachloroethylene by iron sulfide. *Environ. Sci. Technol.* **1998**, *32*, 1276–1284.
- (6) Butler, E. C.; Hayes, K. F. Effects of solution composition and pH on the reductive dechlorination of hexachloroethane by iron sulfide. *Environ. Sci. Technol.* **1999**, *33*, 2021–2027.
- (7) Kennedy, L. G.; Everett, J. W.; Gonzales, J. Assessment of biogeochemical natural attenuation and treatment of chlorinated solvents, Altus AFB, Altus, Oklahoma. *J. Contam. Hydrol.* **2006**, *83*, 221–236.
- (8) Kennedy, L. G.; Everett, J. W.; Becvar, E.; DeFeo, D. Field-scale demonstration of induced biogeochemical reductive dechlorination at Dover AFB, Dover, Delaware. *J. Contam. Hydrol.* **2006**, *88*, 119–136.
- (9) Shen, H.; Wilson, J. T. Trichloroethylene removal from groundwater in flow-through columns simulating a permeable reactive barrier constructed with plant mulch. *Environ. Sci. Technol.* **2007**, *41*, 4077–4083.
- (10) Herbert, R. B.; Benner, S. G.; Blowes, D. W. Solid phase iron-sulfur geochemistry of a reactive barrier for treatment of mine drainage. *Appl. Geochem.* **2000**, *15*, 1331–1343.
- (11) Roh, Y.; Lee, S. Y.; Elless, M. P. Characterization of corrosion products in the permeable reactive barriers. *Environ. Geol.* **2000**, *40*, 184–194.
- (12) Phillips, D. H.; Gu, B. W. D. B.; Roh, Y.; Liang, L.; Lee, S. Y. Performance evaluation of a zerovalent iron reactive barrier: Mineralogical characteristics. *Environ. Sci. Technol.* **2000**, *34*, 4169–4176.
- (13) Benner, S. G.; Blowes, D. W.; Gould, W. D.; Herbert, D. H.; Ptacek, C. J. Geochemistry of a permeable reactive barrier for metals and acid mine drainage. *Environ. Sci. Technol.* **1999**, *33*, 2793–2799.
- (14) Lu, X.; Wilson, J. T.; Shen, H.; Henry, B. M.; Campbell, D. H. Remediation of TCE-contaminated groundwater by a permeable reactive barrier filled with plant mulch (Biowall). *J. Environ. Sci. Health A* **2008**, *43*, 24–35.
- (15) Weerasooriya, R.; Dharmasena, B. Pyrite-assisted degradation of trichloroethylene (TCE). *Chemosphere* **2001**, *389*–396.

- (16) Lee, W.; Batchelor, B. Abiotic reductive dechlorination of chlorinated ethylenes by iron-bearing soil minerals. 1. Pyrite and magnetite. *Environ. Sci. Technol.* **2002**, *36*, 5147–5154.
- (17) Kostka, J. E.; Luther, G. W. Partitioning and speciation of solid phase iron in saltmarsh sediments. *Geochim. Cosmochim. Acta* **1994**, *58*, 1701–1710.
- (18) Wilkin, R. T.; Bischoff, K. J. Coulometric determination of total sulfur and reduced inorganic sulfur fractions in environmental samples. *Talanta* **2006**, *70*, 766–773.
- (19) Rickard, D. The solubility of FeS. *Geochim. Cosmochim. Acta* **2006**, *70*, 5779–5789.
- (20) Berner, R. A. Sedimentary pyrite formation. *Am. J. Sci.* **1970**, *268*, 1–23.
- (21) Burton, E. D.; Phillips, D. Reactive sulfide relationships with trace metal extractability in sediments from southern Moreton Bay. *Aus. Mar. Pollut. Bull.* **2005**, *50*, 589–608.
- (22) Pyzik, A. J.; Sommer, S. E. Sedimentary iron monosulfides: Kinetics and mechanisms of formation. *Geochim. Cosmochim. Acta* **1981**, *45*, 687–698.
- (23) Morse, J. W.; Cornwell, J. C. Analysis and distribution of iron sulfide minerals in recent anoxic sediments. *Mar. Chem.* **1987**, *22*, 55–69.
- (24) Morse, J. W.; Rickard, D. Chemical dynamics of sedimentary acid volatile sulfide. *Environ. Sci. Technol.* **2004**, *38*, 131A–136A.
- (25) Huerta-Diaz, M. A.; Morse, J. W. A quantitative method for determining trace metal concentrations in sedimentary pyrite. *Mar. Chem.* **1990**, *29*, 119–144.
- (26) Rickard, D. Kinetics of pyrite formation by the H₂S oxidation of Fe(II) monosulfide in aqueous solutions between 25 and 125°C: the rate equation. *Geochim. Cosmochim. Acta* **1997**, *61*, 115–134.
- (27) Wilkin, R. T.; Barnes, H. L. Pyrite formation by reactions of iron monosulfides with dissolved inorganic and organic sulfur species. *Geochim. Cosmochim. Acta* **1996**, *60*, 4167–4179.
- (28) Canfield, D. E.; Thamdrup, B.; Fleischer, S. Isotopic fractionation and sulfur metabolism by pure and enrichment cultures of elemental sulfur-disproportionating bacteria. *Limnol. Oceanogr.* **1998**, *43*, 253–264.
- (29) Butler, I. B.; Rickard, D. Framboidal pyrite formation via the oxidation of iron(II) monosulfide by hydrogen sulfide. *Geochim. Cosmochim. Acta* **2000**, *64*, 2665–2672.
- (30) Schoonen, M. A. A.; Barnes, H. L. Reactions forming pyrite and marcasite from solution: II. via FeS precursors below 100° C. *Geochim. Cosmochim. Acta* **1991**, *55*, 1505–1514.
- (31) Rickard, D.; Luther, G. W. Kinetics of pyrite formation by the H₂S oxidation of iron(II) monosulfide in aqueous solutions between 25 and 125° C: the mechanism. *Geochim. Cosmochim. Acta* **1997**, *61*, 135–147.

ES8010354